Tissue Engineering Scaffolds Based on Photocured Dimethacrylate Polymers for in Vitro Optical Imaging

Forrest A. Landis,*,† Jean S. Stephens, James A. Cooper, Marcus T. Cicerone, and Sheng Lin-Gibson*

Polymers Division, National Institute of Standards and Technology, Gaithersburg, Maryland 20899-8543

Received January 17, 2006; Revised Manuscript Received March 13, 2006

Model tissue engineering scaffolds based on photocurable resin mixtures with sodium chloride have been prepared for optical imaging studies of cell attachment. A photoactivated ethoxylated bisphenol A dimethacrylate was mixed with sieved sodium chloride (NaCl) crystals and photocured to form a cross-linked composite. Upon soaking in water, the NaCl dissolved to leave a porous scaffold with desirable optical properties, mechanical integrity, and controlled porosity. Scaffolds were prepared with salt crystals that had been sieved to average diameters of 390, 300, 200, and 100 μm, yielding porosities of approximately 75 vol %. Scanning electron microscopy and X-ray microcomputed tomography confirmed that the pore size distribution of the scaffolds could be controlled using this photocuring technique. Compression tests showed that for scaffolds with 84% (by mass fraction) salt, the larger pore size scaffolds were more rigid, while the smaller pore size scaffolds were softer and more readily compressible. The prepared scaffolds were seeded with osteoblasts, cultured between 3 and 18 d, and examined using confocal microscopy. Because the cross-linked polymer in the scaffolds is an amorphous glass, it was possible to optically image cells that were over 400 μm beneath the surface of the sample.

1. Introduction

The use of synthetic polymeric scaffolds in tissue engineering applications offers new opportunities for the restoration of damaged bone tissue. With these materials, it is important to understand the relationships between the three-dimensional structure of the scaffolds and the response of the cells within the material. Optical microscopy techniques, such as confocal microscopy and optical coherence tomography,[1−6] have been shown to be useful in the examination of the three-dimensional structure of cellular tissues. These imaging techniques are somewhat less useful when applied to many synthetic polymer scaffolds due to the dense and opaque nature of the materials. Synthetic scaffolds with high optical transparency would be desirable for these types of studies.

Many of the synthetic polymeric materials currently used in tissue engineering medical products (TEMPs) for bone replacement applications, such as poly(lactic acid), copolymers of poly(lactic acid) with poly(glycolic acid), and poly(ϵ-caprolactone), are not ideal for optical imaging analysis. The crystalline forms of these polyesters contain crystallites that scatter light and limit the ability to image deep beneath the surface of the scaffold. While the amorphous samples of these polyesters are more transparent, it can be difficult to prepare scaffolds from these materials with good mechanical integrity at the higher end of the porosity range (>85 vol %) where the scaffolds are typically studied.

For our microscopy studies, the ideal tissue engineering scaffold polymer would need to meet several criteria: (1) a low degree of crystallinity to minimize scattering and improve the penetration of visible and near-infrared light, (2) good mechanical integrity, (3) well-defined porosity, pore size, and pore interconnectivity, (4) good cell adhesion and growth in the scaffold, (5) not autofluorescent or readily stained by fluorophores, and (6) hydrolytically stable over several months in cell growth media. To meet these criteria, we have been developing salt-leached tissue engineering scaffolds based on photo-cross-linkable ethoxylated bisphenol A dimethacrylate (EBPADMA) monomers. These monomers are used extensively in the formulation of the matrix material in dental restorative composites,[7] and have been approved for use by the Food and Drug Administration. After curing, the neat EBPADMA resin has ambient properties similar to those of poly(methyl methacrylate) in that it is a rigid, optically transparent polymeric glass. It should be noted that the focus of this study is the development of scaffolds which simulate the porous morphology of bone and have properties which are ideal for optical microscopy imaging and cell activity studies. The in vivo application of scaffolds based on this class of dimethacrylate polymers has not been examined in this study and will be left to future research. The use of photopolymerized polymers to make tissue engineering scaffolds has been reported previously;[8] however, most often, these scaffolds are flexible hydrogels for applications in soft tissue restoration such as cartilage and internal organs.[9] While a few biodegradable photocured polymers for rigid bone replacement applications have been developed,[10−15] these materials are not readily available and most do not meet our needs for optical imaging and cell culture studies, particularly with regard to their optical transparency.

In this study, we report a process to prepare model tissue engineering scaffolds with controlled porosity and pore sizes based on the photopolymerization of a commercially available dimethacrylate monomer in the presence of sodium chloride crystals (porogen). After the photo-cross-linking process, the composite was soaked in water to dissolve the salt and leave a porous scaffold. The porous structure of the scaffolds was characterized using scanning electron microscopy (SEM) and X-ray microcomputed tomography, and the mechanical proper-

* To whom correspondence should be addressed. E-mail: fal100@psu.edu (F.A.L.), slgibson@nist.gov (S.L.-G.).

† Current address: Department of Chemistry, Penn State York, York, PA 17403.

10.1021/bm0600466
Published on Web 04/25/2006

ties were determined using uniaxial compression testing. These scaffolds were also seeded with osteoblasts (cells which deposit bone matrix that calcifies to become new bone) and examined using optical confocal fluorescence microscopy to evaluate the depth of penetration, the cell attachment and morphology within the scaffolds, and the spatial distribution of the cells throughout the scaffolds. These materials will be used for an upcoming study utilizing optical coherence microscopy to examine the relationships between the 3-dimensional structure of the scaffold and the cell response.

2. Materials and Methods

2.1. Materials. Certain equipment, instruments or materials are identified in this paper to adequately specify the experimental details. Such identification does not imply recommendation by the National Institute of Standards and Technology, nor does it imply the materials are necessarily the best available for the purpose. EBPADMA (degree of ethoxylation ~6) was obtained from Esstech Inc. The photoinitiator system of camphorquinone (CQ) and ethyl 4-*N*,*N*-dimethylaminobenzoate (4E) was purchased from Aldrich Corp. All reagents were used as received. The resin was activated for blue light photopolymerization with 0.2% CQ and 0.8% 4E (by mass) and stored in the dark until use. Sodium chloride crystals (from Mallinckrodt Baker, Inc.) were ground into smaller particles using a mortar and pestle and then separated into defined size ranges using brass sieves (Fisher Scientific, Inc.) with nominal sieve openings of 425, 355, 250, 150, and 75 μm.

2.2. Fabrication of EBPADMA Tissue Engineering Scaffolds. The activated EBPADMA (16% by mass) was blended with the sieved salt crystals. The resin/salt mixture was stirred with a spatula for several minutes until the resin had completely wet the salt crystals. The mixture was then packed into a poly(tetrafluoroethylene) (PTFE) frame mold with two glass plates to make a flat plaque that was approximately 8.5 cm^2 by 3 mm thick. A polyester release film was placed between the mixture and the glass plates to prevent adhesion to the glass surface. The entire sandwich mold was held together with binder clips. The sample was cured for 5 min per side in a Dentsply Triad 2000 visible light cure unit with a tungsten halogen light bulb (250 W and 120 V). After curing, the solid sample was removed from the mold and placed in a vacuum oven at 100 °C for 1 h to ensure high conversion of the resin. It should be noted that, for unfilled resins, a cure time of 1 min per side is sufficient to achieve high conversion of the methacrylate end groups on the basis of infrared spectroscopy analysis (FTIR).[16] The more rigorous curing process was applied to the EBPADMA/salt composites because of the potential for light scattering from the salt crystals, which could hinder the curing process. Circular samples (9 mm in diameter) were cut from the flat plaque using a metallic stamp. The disks were soaked in a large volume of deionized water for 48 h with several changes of the water to dissolve the salt porogen and leave a porous polymer scaffold. At the end of the soaking process, treatment of the water with a silver nitrate solution showed no evidence of precipitation of silver chloride indicating that the salt had been removed from the sample. Using densities of 2.165 and 1.198 g/mL for the salt and the cured EBPADMA, respectively, the theoretical porosity of the scaffold, assuming that all the salt was dissolved and no polymer was lost, would be 74 vol %. The actual porosity of the samples was determined using gravimetric analysis of the average mass loss of five identical samples after the soaking process.

The samples for X-ray tomography were prepared in a manner similar to that of the photocured plaques. An 84/16 by mass mixture of the 300 μm average size salt crystals and EBPADMA was prepared and packed into a thin glass tube with a diameter of approximately 3 mm. The glass had been treated with a silanol release agent to facilitate the removal of the sample. The mixture in the glass tube was photocured for 5 min, postcured at 100 °C, and then carefully pushed out of the tube. After soaking in water, a porous rod of scaffold remained which was suitable for X-ray tomography analysis.

2.3. Characterization of Scaffold Morphology. A high-resolution Hitachi S-4700-II field emission scanning electron microscope was used to record electron micrographs of the porous morphology at the surface of the scaffolds. The scaffolds were sputter-coated with gold prior to imaging to enhance image contrast. The SEM images were collected at 5 kV and 15 μA with a working distance of 10 mm. The internal morphology of the scaffold was characterized at Microphotonics, Inc. (Allentown, PA) using a Skyscan 1072 X-ray microcomputed tomography instrument (microCT) with a 100 kV X-ray tube. The pixel size for the scan was 4.5 μm. The sample was rotated through 180°, taking a projection every 0.45°. The tube was set at 40 kV and 98 μA to increase the contrast and to reduce the spot size to 5 μm. After completion of the *xy* scans, 975 slices were reconstructed for data analysis using NRecon software for cone beam reconstruction. Three-dimensional image construction of the *xy* microCT images was performed using an in-house software program that is currently being developed. The images were generated by applying 3D filtering and isosurface algorithms to the data on the 3D grid points. Minor smoothing and data reduction were applied to make the 3D surface models manageable in an interactive immersive visualization environment. The 3D software package is a combination of custom software, components of the OpenDX package, and DIVERSE.

2.4. Mechanical Properties of Scaffolds. The compressive strength of the scaffolds was determined using an ELF 3200 mechanical analyzer (EnduraTec, Inc.) with a 40 N load cell. The disk-shaped samples (approximately 9 mm in diameter by 3 mm in height) were compressed at a rate of 50 μm/s, and the load value was measured four times per second. The compressive strength and modulus of the samples were calculated in a manner similar to that of ASTM method D 1621-04a;[17] however, for the compressive strength calculation, it was not possible to achieve a 10% strain before the load cell reached its maximum due to the rigidity of some of the samples. For our experiments, the compressive strength was determined at a strain value of 7% of the initial sample thickness. The compressive modulus was calculated from the initial cross-sectional area of the sample and the slope of the first linear region after the initial upturn in the stress/strain curve. The reported compression values were an average of values of three samples for each pore size with 1 standard deviation of uncertainty.

2.5. Cell Seeding and Staining of EBPADMA Scaffolds. MC3T3-E1 subclone 4 murine osteoblast cell line was purchased from the American Type Culture Collection (ATCC, Arlington, VA). Cells were cultured in 75 cm^2 tissue culture flasks using cell growth medium and maintained at 37 °C in a humidified incubator at 5% (by volume) CO_2 atmosphere. The cell growth medium was composed of α minimum essential medium (α-MEM) (Cambrex/BioWhitaker, Walkersville, MD), 10% fetal bovine serum (FBS) (Gibco/Invitrogen Corp., Grand Island, NY), 1% L-glutamine (Cambrex/BioWhitaker), 1% sodium pyruvate (Cambrex/BioWhitaker), and 1% antibiotics (penicillin/streptomycin) (Fisher Scientific, Pittsburgh, PA). The medium was replaced every 3 d, and cells at passages 4−7 were used for this study.

Prior to cell seeding, the scaffolds were sterilized using 70% ethanol and allowed to dry overnight. The scaffolds were irradiated with ultraviolet (UV) light for 15 min on each side, rinsed three times with sterile α-MEM, and then incubated at 37 °C for 30 min in cell growth medium. The excess medium was removed, and each scaffold was maintained in 1 well of a 12-well plate. The cells were seeded dropwise onto the scaffolds at densities of 1×10^6 cells per scaffold for the 3 d trial and 0.25×10^6 cells per scaffolds for the 3, 7, and 18 d trials. Once the cells were seeded, they were placed in the 37 °C incubator and allowed to attach for 1 h. The scaffolds were then covered in cell growth medium, which was exchanged every 3 d.

At each time point (3, 7, and 18 d) the appropriate scaffolds were removed from the incubator. The scaffolds were rinsed three times in phosphate-buffered saline (PBS; 3×) to remove excess media. The cells were then fixed to the scaffolds in 4% paraformaldehyde for 20 min at room temperature. The paraformaldehdye was removed, and the scaffolds were rinsed with PBS 3×. The cells were then permeablized

Table 1. Sample Nomenclature and Porosity of EBPADMA Photoscaffolds[a]

sample	sieve grid range (μm)	app av salt cryst size (μm)	measd vol % porosity by mass loss
EBPADMA-100	150−75	100	81.5 ± 1.5
EBPADMA-200	250−150	200	78.0 ± 1.5
EBPADMA-300	350−250	300	75.2 ± 0.8
EBPADMA-390	425−350	390	73.4 ± 1.2

[a] The values are calculated from the average of five samples, and the error corresponds to 1 standard deviation of the data set.

with 0.1% Triton X for 10 min at room temperature. The excess Triton X was removed, and the scaffolds were rinsed with PBS 3×. The cells were stained with Sytox Green (Molecular Probes) at a 1:5000 dilution in PBS for 10 min. Sytox Green is a nucleic acid stain, which was used to mark cell locations within the scaffolds. The scaffolds were again rinsed with PBS 3× to remove excess Sytox Green. Some samples were additionally labeled with Alexa Fluor 546 Phalloidin (Molecular Probes) for actin and for the investigation of cell spreading and morphology. The Alexa Fluor 546 Phalloidin was used in a 40× dilution in PBS and was placed on the samples for 1 h at room temperature. The samples were rinsed with PBS 3× and were ready for imaging.

2.6. Microscopy for Cell Distribution. Confocal optical microscopy analysis of the cultured and stained scaffolds was carried out using a Zeiss LSM 510 laser scanning confocal microscope with a 1 Airy unit pinhole in reflectance mode. A 5× magnification objective was used to cover a broad field of view (approximately 2 mm) and encompass several of the 100−400 μm size pores within the scaffold in a single image. A 488 nm laser was used in simple reflection to examine the scaffold structure while the fluorescence of the incorporated Sytox Green nuclear stain from the 488 nm beam was passed through a 515 nm long-pass filter to determine the location of the stained cells within the scaffold. For the higher detail images of the scaffold with both the nuclear and actin stains, a 50× objective and a 505−550 nm band-pass filter were employed to examine the fluorescence of the stained osteoblast nuclei, while a 560 nm long-pass filter was used to obtain the fluorescence signal of the stained actin filaments in the cells.

3. Results and Discussion

3.1. Porosity of EBPADMA Scaffolds. In this research, we report a process to prepare model tissue engineering scaffolds based on the photopolymerization of a dimethacrylate monomer (EBPADMA) in the presence of sodium chloride crystals. After the photo-cross-linking process, the salt was removed from the composite by soaking in water to leave a porous scaffold material. The scaffold fabrication procedure involved two simple steps, photopolymerization and salt leaching, rendering it facile, rapid, and easily achievable. Unlike scaffolds prepared by other techniques (e.g., freeze-drying, solvent casting, or liquid−liquid-phase separation),[18] the current process does not require any harmful solvents, thereby reducing the potential for toxic reagents to leach out over time. In addition, it is often difficult to control the pore size and porosity of the scaffolds prepared from these other techniques. Throughout this study, the individual scaffolds prepared will be referred to as EBPADMA-followed by the average size of the salt crystals in micrometers incorporated into the formulation (e.g., EBPADMA-300). Table 1 summarizes the estimated size of the salt crystals based on the sieve mesh sizes and the calculated volume percent porosity of the photocured scaffolds determined by gravimetric analysis. The measured values of the porosity were near the theoretical value of 74% for the scaffolds prepared with the larger crystal sizes (e.g., 300 and 390 μm); however, as the average size of the crystals was reduced, the porosity of the scaffold increased above the expected value. As will be described in detail in the next few sections, the scaffolds prepared with the small salt crystal sizes were less robust; therefore, it is likely that small pieces of material near the surface of the scaffold were broken off during the soaking/stirring process. This greater porosity could also be attributed to agglomeration of the smaller salt crystals, allowing for small polymer domains to be unattached to the bulk scaffold during the photocuring process. When the composite was soaked in water, these isolated domains could have been washed out, causing an increase in the porosity. Last, it is possible that the aggregation of the smaller salt particles could have hindered the penetration of light, causing incomplete curing of the material. This uncured resin would then be removed from the scaffold during the salt leaching process, resulting in an increase in the porosity relative to the expected result. However, FTIR measurement of the salt-leached scaffolds showed the degree of methacrylate conversion for scaffolds of

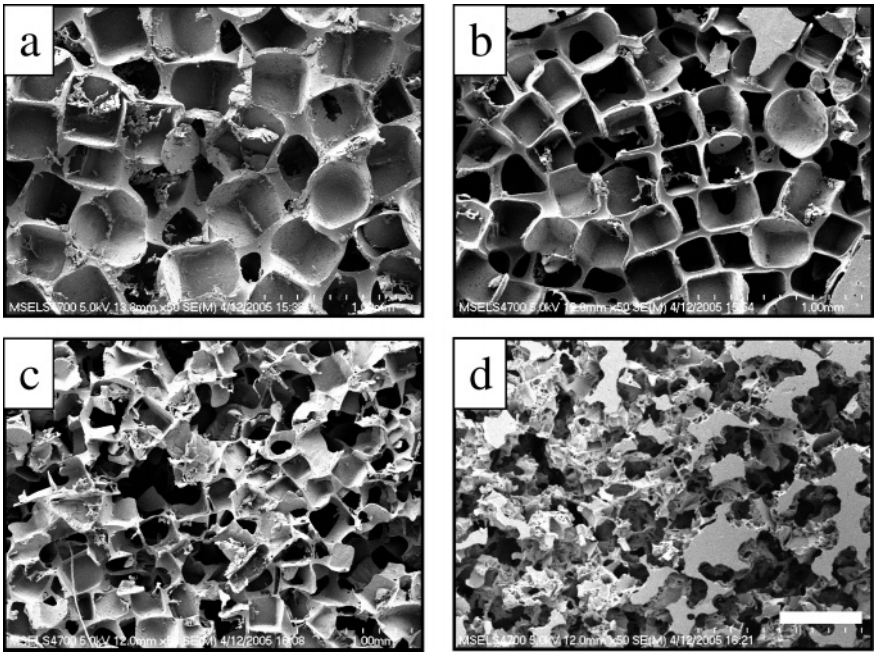

Figure 1. Scanning electron micrographs of the surface of (a) EBPADMA-390, (b) EBPADMA-300, (c) EBPADMA-200, and (d) EBPADMA-100. The scale bar represents 500 μm and applies to all of the images.

all pore sizes to be comparable to that of a highly cured bulk resin sample. Since the amount of partially cured resin, which could not be washed out, was not significant, it is unlikely that free, unreacted monomer was present in an appreciable amount.

3.2. Imaging of EBPADMA Scaffold Morphology. SEM micrographs of the surface of the photocured EBPADMA scaffolds prepared with the variously sized salt crystals are shown in Figure 1. It is apparent from these images that the pore morphology is more homogeneous for those scaffolds prepared with larger crystal sizes and more heterogeneous for those scaffolds prepared with smaller crystal sizes. The structure of the scaffolds prepared with the larger salt crystals is a close replication of the initial polymer/salt blend structure and is open and continuous with roughly cubic pores at approximately the same size as the salt crystals used in the formulation for the scaffolds (Figure 1a−c). However, as the average size of the salt crystals decreased, the pores became less cubic in shape and the dispersity of pore sizes within the scaffold increased (EBPADMA-100 in Figure 1d). This change in the shape of the pores can be accounted for with a few possible explanations. First, to make the smallest salt crystal sizes (100 μm), it was necessary to grind the crystals into a fine powder unlike the larger salt crystals (200, 300, and 390 μm), which had a more granular texture. Optical microscopy of individual ground salt crystals on a glass slide confirmed that the cubic structure of the crystals was broken down, which would result in scaffolds with less cubic pores. The second possibility of this irregular pore structure is that these smaller salt crystals have a much larger overall surface area when compared to large crystals. When the same amount of resin is used, inefficient wetting of the smaller crystals could occur, leading to salt aggregation and the formation of irregular shapes when washed from the scaffold. This would change the distribution of pore sizes due to the greater diversity in the size of the salt aggregates. Finally, as previously discussed, it is possible that, during the soaking process, polymer trapped in salt clusters is washed out, creating the larger pore sizes. This is consistent with the SEM micrograph (Figure 1d) and the observed deviation from the expected porosity. It is reasonable to conclude that the pore structure of the scaffold could be better optimized using an alternative porogen than NaCl with a more regular structure particularly at the smaller particle size range. While the morphology of the salt-leached photoscaffolds is not perfect, the SEM images indicate that the current scaffold fabrication process leads to adequate control of the average pore sizes and structures. The ability to manipulate the pore structure within the scaffolds is important for studies investigating the cell response to the 3-dimensional structure of these scaffolds.

Figure 2a shows an image of the internal structure of the EBPADMA-300 scaffold obtained using microCT analysis. MicroCT is a technique that uses X-ray scattering and computer analysis to reconstruct a single tomographic slice (*xy*) of the internal morphology of the scaffold as the sample is rotated 180° within the beam. By moving in the *z* direction, it is possible to obtain several image slices throughout the scaffold that can then be combined to form a 3-dimensional representation of the morphology of the sample (Figure 2b). These microCT images showed no evidence of residual salt within the scaffold, indicating that the leaching process was complete. In addition, the internal structure of the scaffold was similar to the cubic pore morphology observed at the surface in the SEM images. The internal pore structure appears to be highly interconnected and continuous, which is an important factor in cell penetration and in diffusion of nutrients and waste products through the scaffold. The images obtained from microCT analysis of the salt scaffolds are useful for the analysis of such scaffold characteristics as porosity, pore size distribution, and mechanical properties, which will be examined in future research.

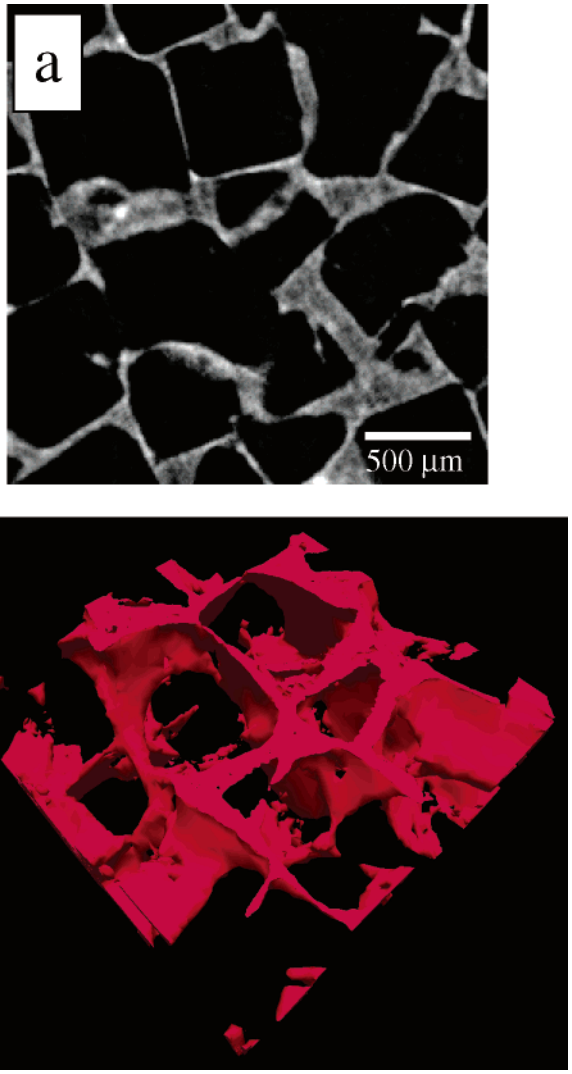

Figure 2. (a) A single X-ray microcomputed tomography slice showing the porous interior of an EBPADMA-300 scaffold and (b) a 3D compilation of 100 slices of the X-ray micrographs.

3.3. Compressive Strength of EBPADMA Scaffolds. The mechanical properties of the photoscaffolds as a function of salt porogen size were determined using uniaxial compression testing. Figure 3 shows the compressive stress versus strain for the EBPADMA scaffolds prepared with the variously sized salt porogens. The mechanical response of all the samples exhibited a flat initial response followed by a sharp upturn into a linear region. This initial response is due to the compression of the rough surface regions of the scaffold, and the upturn and linear sections correspond to the "bulk" compressive properties of the scaffold. It is interesting to note that the length of the region in the traces from the initial contact to the upturn increases as the size of the pores in the scaffold increases. This is consistent with the SEM micrographs, which show the scaffolds with larger pores have increased surface roughness and, therefore, would take longer to compress before reaching the bulk scaffold compression properties. The shape of the stress versus strain curve after the initial slope is also affected by the salt crystal size. For scaffolds containing larger salt sizes (i.e., 390 and 300 μm), the stress continues to increase to the limit of the load cell. For the scaffold prepared with the 200 μm size salt crystals,

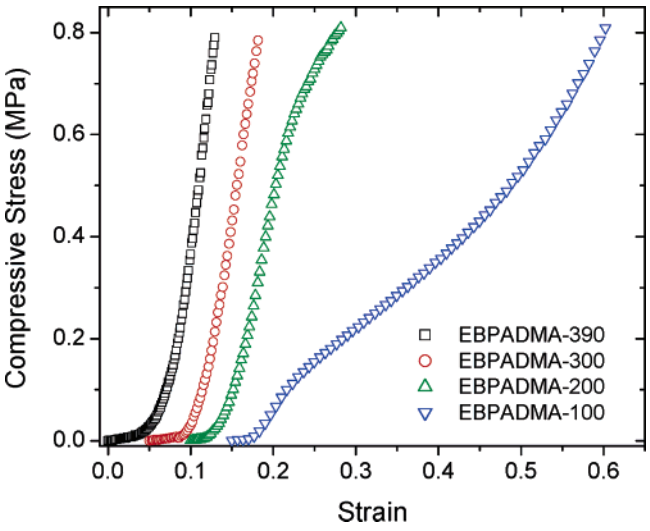

Figure 3. Mechanical compressive response of EBPADMA scaffolds with varying pore sizes. For clarity, the curves are horizontally shifted by a strain of 0.05 with respect to the previous curve.

Table 2. Compressive Mechanical Properties of EBPADMA Scaffolds[a]

sample	compressive strength at 7% strain (MPa)	compressive modulus (MPa)
EBPADMA-100	0.15 ± 0.02	2.4 ± 0.9
EBPADMA-200	0.52 ± 0.10	7.6 ± 1.2
EBPADMA-300	0.70 ± 0.03	10.5 ± 1.4
EBPADMA-390	0.88 ± 0.09	13.4 ± 1.8

[a] The values are calculated from the average of three samples, and the error corresponds to 1 standard deviation of the data set.

a yielding-like behavior is observed at a strain of 0.12 (shown in Figure 3 on the shifted curve at approximately 0.22). The scaffold prepared with the smallest size salt crystal exhibits a complex compression behavior when compared to the other scaffolds. In this small-pore scaffold, a strong yielding behavior is observed at relatively low strain values.

The values of the compressive strength and modulus (Table 2) were calculated from the stress/strain curves shown in Figure 3. Both the compressive strength and modulus increased as the size of the pores increased. The mechanical properties increased by a factor of 5 when comparing the scaffolds with the smallest pore sizes to those with the largest pore sizes. Since all scaffolds were made from the same base monomer with a modulus after photocuring of 1.8 GPa,[16] differences in the mechanical properties result from the changes in the structure and density of the scaffolds. As mentioned previously, although this series of scaffolds all had an initial polymer content of 16% by mass, the polymer volume fractions in the resulting scaffolds were slightly different (Table 1). To separate the effects of scaffold structure and density, the modulus and compression strength values were normalized to a common volume fraction. The volume-normalized values show the same trend (i.e., the strength and modulus increase as the salt crystal size increases), indicating that the mechanical properties depend primarily upon the pore structure.

The current study demonstrates that the scaffold mechanical properties can be altered by varying the porogen size used in the scaffold formation. This is consistent with previous findings that contain limited data relating the porogen size to the mechanical properties of the photocured scaffolds designed for bone therapy.[13,19] The mechanical properties of EBPADMA photoscaffolds are quite good. As a comparison, the compressive modulus of trabecular bone (70% porosity) is 100 MPa.[20] The modulus of a polyester (poly(propylene fumarate)) photoscaffold (65% porosity) is reported to be 3.9 MPa.[17] The scaffolds used in the current study, which have a higher porosity (approximately 75%) and a similar pore size, resulted in a maximum compressive modulus of 13.4 MPa. While a direct comparison of the moduli is not possible due to the differences in the porosities, it is apparent that the EBPADMA photoscaffold with a higher porosity exhibits a significantly greater modulus when compared to the polyester photoscaffold. It is reasonable to expect that the difference in elastic modulus would be greater if the porosity were the same. The enhanced mechanical properties are attributed to the chemical structure of the EBPADMA, which contains a rigid bisphenol A backbone, and the higher cross-link density of the EBPADMA scaffolds.

3.4. Imaging of Cell Distribution and Morphology in EBPADMA Scaffolds. The images from the reflectance and fluorescence channels of the confocal microscope are overlaid and shown in Figure 4. All of the images show that the osteoblasts (red, as shown in the image) are dispersed and attached throughout the highly porous scaffold (white). Due to the very rough nature of the surface of the scaffolds, it is difficult to define exactly the location of the surface of the sample. Figure 4a shows a confocal microscopy image taken at approximately the surface of the sample. As the imaging depth is increased, parts b−d of Figure 4 show that cells at depths greater than 400 μm can be observed. (It is very difficult to accurately define and compare the depth to which cells can be examined within porous scaffolds. Factors such as porosity and pore size greatly affect the depth of penetration of visible light. It is, however, expected due to the optical clarity of the neat photocured EBPADMA resin relative to other photocross-linked monomers (i.e., poly(lactic acid), etc.) that the depth of penetration would be greater.) These images were taken with an air objective; however, using an index matching fluid and the appropriate objective, it is possible to remove the interfacial surface scattering arising from the scaffold and observe the fluorescence of the cells throughout the entire scaffold. It should be noted that no significant fluorescence was observed in any of the images from the stained, cell-free scaffold, indicating that the scaffold does not autofluoresce in this wavelength region and does not appear to interact with the Sytox Green (488 nm) or the Alexa Fluor 546 Phalloidin stain. The images in Figure 4 demonstrate that the osteoblasts have penetrated deeply within the scaffold during seeding and incubation, which is an important characteristic for our upcoming imaging studies. The cells appear to maintain healthy morphologies at each of the time points (3, 7, and 18 d), indicating that no cytotoxic soluble molecules are leaching out of the scaffold during the culture process.

Figure 5 shows a high-magnification confocal microscopy image of osteoblasts on an EBPADMA-300 scaffold that have been stained with fluorescent reagents specific for the nuclear DNA (green) and the actin microfilaments of the cytoskeleton (red). Figure 5 illustrates that the cell/scaffold interactions favor a normal cell morphology and that the cells cover the surface of the scaffold. These observations further indicate that the EBPADMA photoscaffolds offer an environment that promotes cell attachment and viability.

4. Conclusion

A technique has been described to prepare model tissue engineering scaffolds that have a porous morphology similar

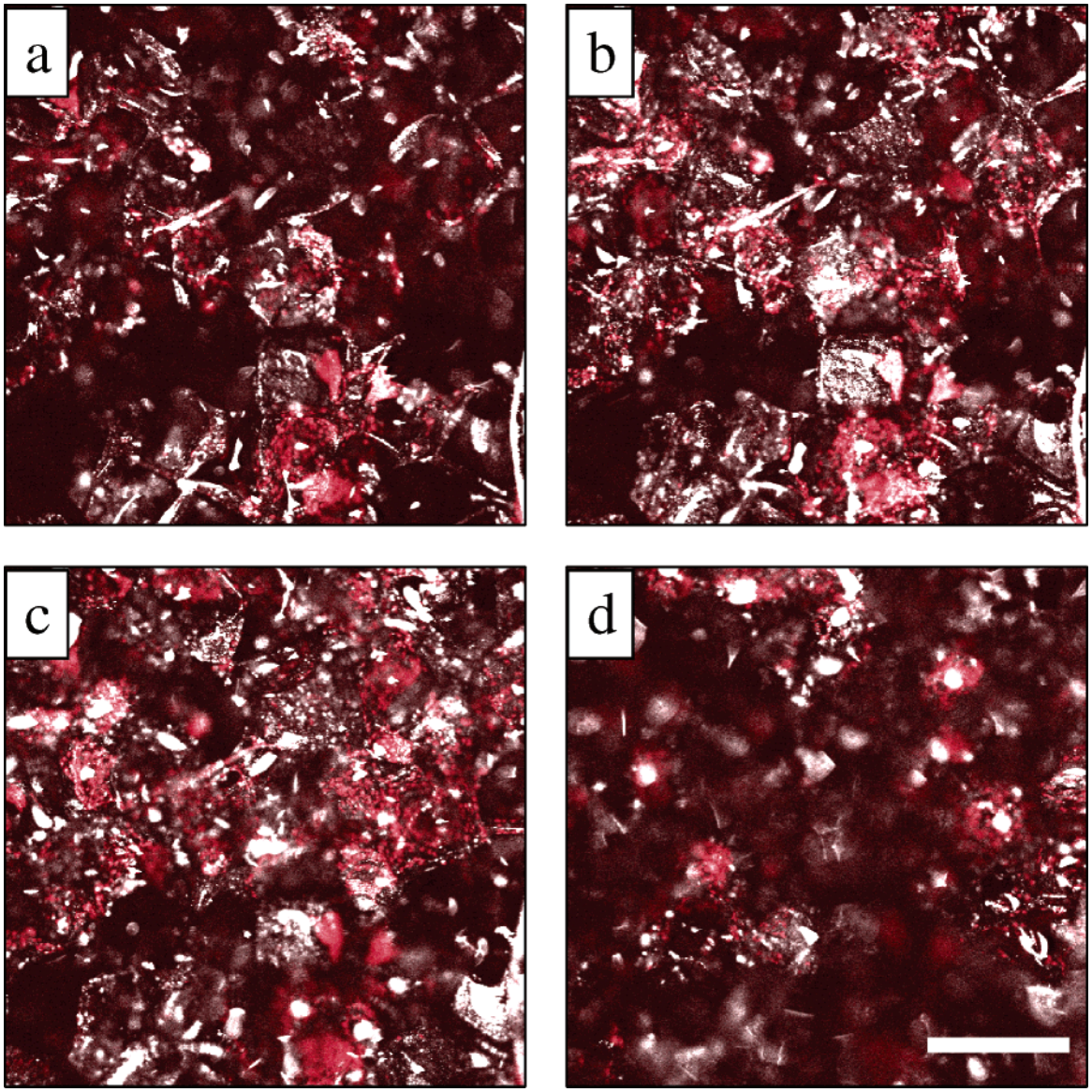

Figure 4. Confocal microscopy images of osteoblasts distributed within an EBPADMA-300 scaffold after 18 d: (a) the surface of the scaffold, (b−d) a depth of (b) 100 μm, (c) 200 μm, and (d) 400 μm below the surface. Cells are labeled red, and the scaffold is shown in white. The scale bar represents 500 μm and applies to all of the images.

to that of bone and are conducive to optical imaging of the cell response within the 3-dimensional construct. The process involved the photocuring of a 16% by mass ethoxylated bisphenol A dimethacrylate monomer with sieved salt crystals. After removal of the salt by soaking in water, a porous scaffold remained with controlled pore size and porosity. Scaffolds were prepared using salt that had been sieved to average diameters in the range of 390−100 μm. Scanning electron microscopy and X-ray microcomputed tomography indicated that the surface and internal morphology of the scaffolds were very similar in size and shape to those of the salt crystals used in the formulation. Calculations based on mass lost during the soaking process indicated that scaffolds made with larger salt crystals approached the calculated theoretical porosity of 74 vol %. As the salt crystal size decreased, however, the scaffolds became slightly more porous and the pore size was more polydisperse.

Compressive mechanical analysis of the scaffolds showed that the mechanical properties of the scaffold can be changed from a rigid, hard material for the scaffolds prepared with the largest salt crystals to a flexible, soft foam for those made with the smallest salt crystals. All of the scaffolds prepared had sufficient mechanical integrity to be utilized in the cell seeding process. Osteoblasts were seeded on the scaffold and cultured up to 18 d. At 3, 7, and 18 d, confocal microscopy imaging showed that the cells were well-distributed throughout the scaffold. Due to the glassy nature of the scaffolds, these materials were more transparent than crystalline polymer based scaffolds that scatter light and limit penetration. Confocal microscopy showed that cells at depths of over 400 μm below the surface of the scaffolds could be imaged. This ability to image cells to high depths will be useful in upcoming studies where we will be examining the relationships between scaffold mesostructure and cell response in static and dynamic cell culture processes.

Acknowledgment. The EBPADMA resins were kindly donated by Esstech, Inc. We acknowledge the NIST/NRC Postdoctoral Fellowship Program for funding. In addition, we thank Drs. Joy P. Dunkers, Joseph M. Antonucci, and Nancy J. Lin for their advice and technical recommendations.

Supporting Information Available. NIR spectra of EBPADMA resins. This material is available free of charge via the Internet at http://pubs.acs.org.

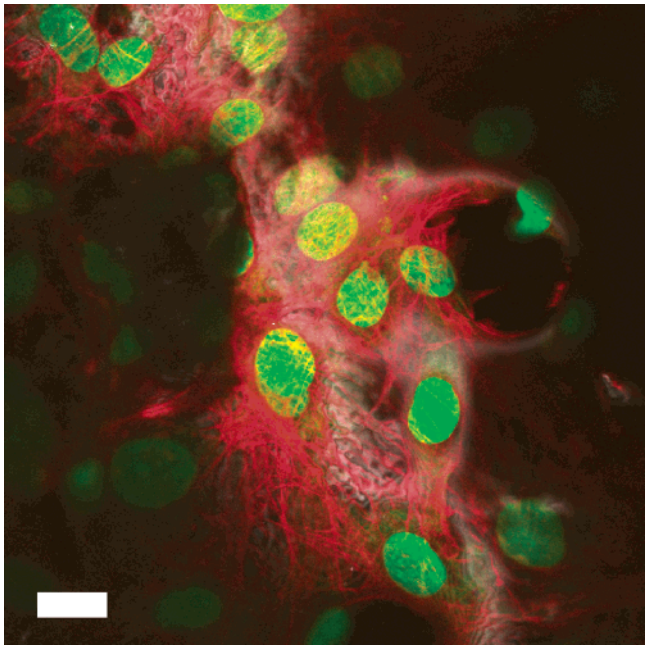

Figure 5. A confocal microscopy image of osteoblasts on an EBPADMA-300 scaffold after 3 d of culture. The cell nuclei are labeled green (Sytox Green), the actin fibers within the cells are labeled red (Alexa Fluor 546 Phalloidin), and the photoscaffold is shown in white. The scale bar represents 20 μm.

References and Notes

(1) Bouma, B. E.; Tearney, G. J. *The Handbook of Optical Coherence Tomography*; Marce-Dekkar, Inc.: New York, 2002.

(2) Huang, D.; Swanson, E. A.; Lin, C. P.; Schuman, J. S.; Stinson, W. G.; Chang, W.; Hee, M. R.; Flotte, T.; Gregory, K.; Puliafito, C. A.; Fujimoto, J. G. *Science* **1991**, *254*, 1178−1181.

(3) Bouma, B. E.; Tearney, G. J. Optical Coherence Microscopy. In *The Handbook of Optical Coherence Tomography*; Bouma, B. E., Tearney, G. J., Eds.; Marce-Dekkar, Inc.: New York, 2002.

(4) Izatt, J. A.; Hee, M. R.; Owen, G. M.; Swanson, E. A.; Fujimoto, J. G. *Opt. Lett.* **1994**, *19*, 590−592.

(5) Landis, F. A.; Cicerone, M. T.; Cooper, J. A.; Stephens, J. S.; Dunkers, J. P. Collinear Optical Coherence and Confocal Fluorescence Microscopy and Its Application to Tissue Engineering. Unpublished work, 2005.

(6) Dunkers, J. P.; Cicerone, M. T.; Washburn, N. R. *Opt. Express* **2003**, *11*, 3074−3079.

(7) Moszner, N.; Salz, U. *Prog. Polym. Sci.* **2001**, *26*, 535−576.

(8) Fisher, J. P.; Dean, D.; Engel, P. S.; Mikos, A. G. *Annu. Rev. Mater. Res.* **2001**, *31*, 171−181.

(9) Bryant, S. J.; Anseth, K. S. *Biomaterials* **2001**, *22*, 619−626.

(10) Anseth, K. S.; Shastri, V. R.; Langer, R. *Nat. Biotechnol.* **1999**, *17*, 156−159.

(11) Burdick, J. A.; Philpott, L. M.; Anseth, K. S. *J. Polym. Sci., Part A: Polym. Chem.* **2001**, *39*, 683−692.

(12) Burdick, J. A.; Frankel, D.; Dernell, W. S.; Anseth, K. S. *Biomaterials* **2003**, *24*, 1613−1620.

(13) Fisher, J. P.; Holland, T. A.; Dean, D.; Engel, P. S.; Mikos, A. G. *J. Biomater. Sci., Polym. Ed.* **2001**, *12*, 673−687.

(14) Fisher, J. P.; Tirnmer, M. D.; Holland, T. A.; Dean, D.; Engel, P. S.; Mikos, A. G. *Biomacromolecules* **2003**, *4*, 1327−1334.

(15) Wang, S. F.; Lu, L. C.; Gruetzmacher, J. A.; Currier, B. L.; Yaszemski, M. J. *Macromolecules* **2005**, *38*, 7358−7370.

(16) Lin-Gibson, S.; Landis, F. A.; Drzal, P. L. *Biomaterials* **2006**, *27*, 1711−1717.

(17) *ASTM Book of Standard*; American Society for Testing and Materials: West Conshohocken, PA, 2004; Vol. 08.01 [D 1621-04a].

(18) Ma, P. X. *Mater. Today* **2004**, *7*, 30−40.

(19) Fisher, J. P.; Holland, T. A.; Dean, D.; Mikos, A. G. *Biomacromolecules* **2003**, *4*, 1335−1342.

(20) Panjabi, M. M.; White, A. A. *Biomechanics in the Musculoskeletal System*; Churchill Livingstone: Philadelphia, PA, 2001; p 174.

BM0600466